DTU Library

Hubbard-U corrected Hamiltonians for non-self-consistent random-phase approximation total-energy calculations
A study of ZnS, TiO2, and NiO

Patrick, Christopher; Thygesen, Kristian Sommer

Hubbard-*U* corrected Hamiltonians for non-self-consistent random-phase approximation total-energy calculations: A study of ZnS, TiO₂, and NiO

Christopher E. Patrick and Kristian S. Thygesen

Center for Atomic-Scale Materials Design (CAMD), Department of Physics, Technical University of Denmark,
DK-2800 Kongens Lyngby, Denmark

In non-self-consistent calculations of the total energy within the random-phase approximation (RPA) for electronic correlation, it is necessary to choose a single-particle Hamiltonian whose solutions are used to construct the electronic density and noninteracting response function. Here we investigate the effect of including a Hubbard-*U* term in this single-particle Hamiltonian, to better describe the on-site correlation of 3*d* electrons in the transition metal compounds ZnS, TiO₂, and NiO. We find that the RPA lattice constants are essentially independent of *U*, despite large changes in the underlying electronic structure. We further demonstrate that the non-self-consistent RPA total energies of these materials have minima at nonzero *U*. Our RPA calculations find the rutile phase of TiO₂ to be more stable than anatase independent of *U*, a result which is consistent with experiments and qualitatively different from that found from calculations employing *U*-corrected (semi)local functionals. However we also find that the +*U* term cannot be used to correct the RPA's poor description of the heat of formation of NiO.

I. INTRODUCTION

Transition metal compounds (TMCs), particularly in their nanostructured form, find applications in a diverse range of technological fields including photovoltaics and photocatalysis, magnetic storage, and phosphorescent imaging [1–4]. Rational optimization of TMCs at the nanoscale requires an atomistic, quantum-mechanical description of these materials, which in principle can be provided by density-functional theory (DFT) [5]. Unfortunately, the most widely used approximations to the DFT exchange-correlation (XC) energy, namely the local-density and generalized-gradient approximations (LDA/GGA), have difficulty in describing the localized *d* electrons of the transition metals [6].

This difficulty has been ascribed to the unphysical self-interaction experienced by the electrons within the LDA/GGA, and a number of methods have been proposed to overcome it [6]. One popular method is to supplement the LDA/GGA XC potential with orbital-dependent *U* terms, designed to more accurately describe the on-site correlation of the *d* electrons [7]. Such "Hubbard-*U*" corrections have been found to give an improved description of the properties of TMCs like NiO [7–11].

A less widely investigated approach to improving the LDA/GGA description of the TMCs is to obtain the XC energy as a combination of the "exact" Hartree-Fock exchange energy (EXX) and the correlation energy calculated within the random-phase approximation (RPA) [12,13]. Such a scheme should benefit from the EXX correction of self-interaction [6], and also from the nonlocal and dynamical description of correlation provided by the RPA. Specifically, the RPA correlation energy should capture long-range dispersive interactions that are missing in the Hubbard-*U* corrections [12,13]. Recent work has demonstrated the good performance of the RPA + EXX approach for calculating the formation energies and relative stabilities of transition metal oxides [14–17].

From the point of view of performing predictive calculations, the RPA + EXX scheme carries the additional advantage of being essentially parameter-free. However, it is important to note that the most well-documented successes of this scheme—for instance, in describing nonlocal correlation in weakly bonded systems, describing chemisorption and bonding in solids, or in the TMC examples above—were performed non-self-consistently [18–22]. That is, the XC potential felt by the noninteracting electrons was not the functional derivative of the XC energy, at variance with the standard Kohn-Sham (KS) formulation of DFT [23].

Although self-consistent RPA calculations have been demonstrated, they remain a significant technical challenge [24–28]. Therefore a key question to ask is how the choice of XC potential in the single-particle Hamiltonian affects the total energy calculated in a non-self-consistent RPA + EXX scheme. An analogy can be drawn with one-shot calculations of quasiparticle energies within the *GW* approximation (*G*₀*W*₀), where the Green's function and screened Coulomb interaction are usually constructed from LDA/GGA wave functions [29]. Here it has been established that the calculated quasiparticle energies (e.g., the band gap) can depend strongly on the XC potential used in the single-particle Hamiltonian [30–33].

Studies which have explored this aspect for RPA + EXX total-energy calculations have usually focused on the differences between LDA and GGA or on the effect of including Hartree-Fock exchange [22,34–38]. In most cases, the initial choice of XC potential has been found to play only a minor role; a notable exception is the study of cerium in Ref. [39], and of molecular dissociation in Refs. [40,41]. However, for TMCs it is natural to investigate the effect on the RPA + EXX total energy of adding Hubbard-*U* corrections to the XC potential. Since such corrections can significantly change the character of the single-particle wave functions and their energy eigenvalues, one might expect to observe a dependence of the RPA + EXX total energy on the parameter *U*. Indeed, one might even hope that including Hubbard-*U* corrections in the XC potential might improve the quality of the subsequent RPA + EXX calculation, if the resulting single-particle wave functions are closer to the exact KS

form [16]. On the other hand, it is important to note that the orbital-dependent Hubbard-U corrections are nonlocal, and that the RPA correlation energy is strictly nonvariational with respect to all possible nonlocal XC potentials [42].

Motivated by these considerations, we have performed a systematic study of the effects of Hubbard-U corrections on the non-self-consistent RPA + EXX total energy of TMCs. We present results for ZnS, TiO$_2$, and NiO which, in terms of their $3d$ states, display progressively more complex electronic structure. From the total energies we obtain lattice constants as a function of the U parameter within the RPA approximation for the correlation energy, and compare the results to non-self-consistent EXX, self-consistent GGA + U or LDA + U, and experiment. We also consider the energetics of the technologically important TiO$_2$ polymorphs of anatase and rutile, and the heats of formation of TiO$_2$ and NiO.

The rest of our paper is organized as follows. In Sec. II we outline the theory of the non-self-consistent RPA + EXX scheme and describe our computational approach. In Secs. III A, III B, and III C we present our results for ZnS, TiO$_2$, and NiO, including our calculations of the phase stability of TiO$_2$ in Sec. III B 3. We provide a detailed analysis of the U dependence of the total energy in Secs. III D and III E, and consider the oxide heats of formation in Sec. III F. We present our conclusions in Sec. IV.

II. THEORY AND COMPUTATIONAL METHODOLOGY

A. Non-self-consistent RPA total energy

We consider the ground-state total energy E_{Tot} of a system of electrons and nuclei, treating the nuclei as classical, stationary particles. Within the adiabatic-connection fluctuation-dissipation formulation of DFT [12,13,43,44], E_{Tot} is decomposed as

$$E_{\text{Tot}} = E_0 + E_{\text{X}} + E_{\text{C}}. \tag{1}$$

The quantity E_0 appearing in Eq. (1) is the total energy neglecting exchange and correlation, given by

$$E_0 = T_s[\{\psi\}] + E_{Ie}[\rho] + E_{\text{Har}}[\rho] + E_{II}, \tag{2}$$

where $\{\psi\}$ denotes the set of single-particle wave functions obtained from solving

$$H^0|\psi_{\nu\sigma}\rangle = \varepsilon_{\nu\sigma}|\psi_{\nu\sigma}\rangle, \tag{3}$$

where H^0 is a single-particle Hamiltonian (Sec. II B). The electronic density ρ is constructed as $\sum_{\nu\sigma} f_{\nu\sigma}|\psi_{\nu\sigma}|^2$, where $f_{\nu\sigma}$ gives the occupation number of the state. For crystalline systems ν is a composite index labeling band index and wave vector, and σ is a spin index (here we assume collinear spin polarization). T_s gives the kinetic energy of the single-particle wave functions, and E_{Ie}, E_{Har}, and E_{II} give the electron-nuclear, electron-electron, and nuclear-nuclear electrostatic interaction energies.

The exchange energy E_{X} is obtained as

$$E_{\text{X}} = -\frac{1}{2} \sum_{\nu_1,\nu_2,\sigma} f_{\nu_1\sigma} f_{\nu_2\sigma} \int d\mathbf{r} \int d\mathbf{r}'$$
$$\times \frac{\psi_{\nu_1\sigma}(\mathbf{r})\psi_{\nu_2\sigma}^*(\mathbf{r})\psi_{\nu_2\sigma}(\mathbf{r}')\psi_{\nu_1\sigma}^*(\mathbf{r}')}{|\mathbf{r} - \mathbf{r}'|}, \tag{4}$$

(Hartree units are used throughout), and the correlation energy E_{C} is expressed as

$$E_{\text{C}} = -\frac{1}{2\pi} \int_0^1 d\lambda \int_0^\infty ds \int d\mathbf{r} \int d\mathbf{r}'$$
$$\times \frac{\chi^\lambda(\mathbf{r},\mathbf{r}';is) - \chi_{\text{KS}}(\mathbf{r},\mathbf{r}';is)}{|\mathbf{r} - \mathbf{r}'|}, \tag{5}$$

where s is a real number representing an imaginary frequency, $\omega = is$. λ is a coupling constant taking values between 0 and 1 which controls the strength of the Coulomb interaction along the adiabatic connection, and defines a Hamiltonian H^λ whose solution yields the exact ground-state electronic density for all λ.

The response functions χ appearing in the integrand of Eq. (5) are related through an integral equation [45]. Within the RPA this equation can be inverted to give $\chi_{\text{RPA}}^\lambda(\omega) = [1 - \lambda\chi_{\text{KS}}(\omega)v_{\text{C}}]^{-1}\chi_{\text{KS}}(\omega)$, where v_{C} is the Coulomb interaction. Integrating over the coupling constant in Eq. (5) and expanding the response function in a plane-wave basis yields the RPA correlation energy [12,13],

$$E_{\text{C}}^{\text{RPA}} = \frac{1}{2\pi} \sum_{\mathbf{q}} \int_0^\infty ds \, \text{Tr}[\ln\{1 - v_{\text{C}}(\mathbf{q})\chi_{\text{KS}}(\mathbf{q},is)\}$$
$$+ v_{\text{C}}(\mathbf{q})\chi_{\text{KS}}(\mathbf{q},is)], \tag{6}$$

where $\mathbf{q}$ is a wave vector in the first Brillouin zone, and the response function is a matrix in the reciprocal lattice vectors $\mathbf{G}$ and $\mathbf{G}'$, with elements given by [46]

$$\chi_{\text{KS}}^{\mathbf{G}\mathbf{G}'}(\mathbf{q},is) = \frac{1}{\Omega} \sum_{\mathbf{k}nn'\sigma} (f_{n\mathbf{k}\sigma} - f_{n'\mathbf{k}+\mathbf{q}\sigma})$$
$$\times \frac{n_{n\mathbf{k},n'\mathbf{k}+\mathbf{q}}^\sigma(\mathbf{G}) n_{n\mathbf{k},n'\mathbf{k}+\mathbf{q}}^{\sigma*}(\mathbf{G}')}{is + \varepsilon_{n\mathbf{k}\sigma} - \varepsilon_{n'\mathbf{k}+\mathbf{q}\sigma}}. \tag{7}$$

Ω is the volume of the primitive unit cell, and the pair density $n_{n\mathbf{k},n'\mathbf{k}+\mathbf{q}}^\sigma(\mathbf{G}) = \langle \psi_{n\mathbf{k}\sigma}|e^{-i(\mathbf{q}+\mathbf{G})\cdot\mathbf{r}}|\psi_{n'\mathbf{k}+\mathbf{q}\sigma}\rangle$.

Setting E_{C} to $E_{\text{C}}^{\text{RPA}}$ in Eq. (1) completes our prescription for a calculation of the RPA total energy $E_{\text{Tot}}^{\text{RPA}}$. The density and response function are constructed from the set of wave functions which solve Eq. (3), and the separate contributions to $E_{\text{Tot}}^{\text{RPA}}$ are evaluated from Eqs. (2), (4), and (6), i.e.,

$$E_{\text{Tot}}^{\text{RPA}} = E_0 + E_{\text{X}} + E_{\text{C}}^{\text{RPA}}. \tag{8}$$

For comparison we also consider the non-self-consistent total energy only including the exact exchange (EXX) contribution,

$$E_{\text{Tot}}^{\text{EXX}} = E_0 + E_{\text{X}}. \tag{9}$$

In passing we point out that by defining E_0 as in Eq. (2) we remove the need to include double-counting corrections in Eqs. (8) and (9) (to be contrasted with, e.g., Eqs. (7) and (27) of Ref. [12]).

B. Single-particle Hamiltonian

The procedure outlined in the previous section of calculating $E_{\text{Tot}}^{\text{RPA}}$ leads to an ambiguity in the definition of the single-particle Hamiltonian H^0. As mentioned above,

the adiabatic connection depends on the exact density being recovered for all values of λ. Equation (3) corresponds to $\lambda = 0$, thus identifying H^0 as the single-particle Hamiltonian which yields the exact density of the system of interacting electrons, i.e., the Kohn-Sham (KS) Hamiltonian with the exact exchange-correlation (XC) potential V_{XC} [23]. One approach therefore would be to use the solutions of this Hamiltonian [Eq. (3)] to compute the contributions $E_0 + E_X$ in Eq. (1), independent of any subsequent approximation used to compute E_C (e.g., the RPA). However, such an approach relies on having the exact V_{XC}, which is unfortunately not known.

An alternative approach is to treat the combined quantity $E_{XC}^{RPA} = E_X + E_C^{RPA}$ as an orbital-dependent XC functional, and use a Kohn-Sham Hamiltonian in Eq. (3) with an XC potential constructed as a functional derivative, $V_{XC}^{scRPA} = \delta E_{XC}^{RPA}/\delta\rho$. This self-consistent (sc) RPA scheme ensures compatibility between the total-energy functional and XC potential [24–28]. In contrast to the non-self-consistent case, in this scheme the RPA is being used to determine H^0 and thus $E_0 + E_X$. Therefore the scRPA scheme can no longer be considered as an approximation to E_C alone. Of course since E_{XC}^{RPA} is nonlocal and energy dependent, it may also be hoped that V_{XC}^{scRPA} might represent a better approximation to the unknown, exact V_{XC} than simpler functionals like the LDA/GGA.

In this work we focus on the first (non-self-consistent) approach, and approximate the exact V_{XC} with one chosen from the class of functionals which include a Hubbard U term. Specifically we supplement standard LDA/GGA XC functionals with the correction derived in Ref. [9],

$$\Delta E_U = \frac{U}{2} \sum_a \text{Tr}(\rho^a - \rho^a\rho^a). \tag{10}$$

The density matrices ρ^a describe the occupation of localized orbitals on atom a, and U controls the strength of the on-site Coulomb interaction incorporating both Hartree (U_H) and exchange (J) contributions, $U = U_H - J$ [9]. The LDA/GGA$+U$ XC potential V_{XC}^U is constructed using Eq. (10) following the scheme described in Refs. [47,48], with the d projectors located on Zn, Ti, and Ni atoms defining the density matrices appearing in Eq. (10) [47]. The single-particle Hamiltonian used in Eq. (3) is thus

$$H^0(U) = [T + V_{Ie} + V_{Har}] + V_{XC}^U, \tag{11}$$

where the operators in the square brackets are obtained as the functional derivative of E_0 [Eq. (2)]. We emphasize that U is considered a free parameter which, for a given choice of LDA or GGA, completely determines H^0 (and thus E_{Tot}^{RPA}) through Eq. (11).

C. Computational details

All calculations were performed within the projected-augmented wave (PAW) formalism [49] of DFT [5,23] as implemented in the GPAW code [47]. The core-valence interaction was described using the 0.9.11271 GPAW datasets, which always treat the $4s$ and $3d$ shells of the transition metals as valence states, and further explicitly include the $3s$ and $3p$ shells for Ti and $3p$ shell for Ni. Exchange and correlation

TABLE I. Size of Γ-centred Monkhorst-Pack grids [52] used in the calculation of EXX total energy and RPA correlation energy for each material.

	$E_0 + E_X$	E_C^{RPA}
ZnS	$10\times10\times10$	$6\times6\times6$
TiO$_2$ (rutile)	$6\times6\times8$	$4\times4\times6$
TiO$_2$ (anatase)	$8\times8\times4$	$6\times6\times4$
NiO[a]	$8\times8\times4$	$8\times8\times4$
Ti	$22\times22\times22$	$12\times12\times12$
Ni	$22\times22\times22$	$14\times14\times14$

[a]$1\times1\times2$ supercell used to describe antiferromagnetic unit cell.

effects were described either within the LDA [50] or GGA (the PBE XC-functional) [51] with the Hubbard-U correction scheme described above [9,47,48].

The electronic wave functions were expanded in plane waves up to a maximum energy of 80 Ry. The wave functions were sampled on the Γ-centred Monkhorst-Pack [52] grids listed in Table I. For the metals, the electronic occupations were modeled with a Fermi-Dirac distribution of width 0.01 eV. The small-wave-vector divergence of the Coulomb interaction was handled with the Wigner-Seitz truncation scheme of Ref. [53] when calculating the exchange energy, and with the perturbation theory approach described in Ref. [46] when calculating the correlation energy.

The response function χ_{KS} was expanded in plane waves up to a maximum energy E_{cut} of 30 Ry. Following previous studies [22,38] we set the number of unoccupied bands used in Eq. (7) equal to the number of plane waves used to describe χ_{KS}, and extrapolated the results obtained at finite E_{cut} (20–30 Ry) to the basis set limit using the power law expression $E_C^{RPA}(E_{cut}) = E_C^{RPA}(\infty) + AE_{cut}^{-3/2}$. The frequency integration in Eq. (6) was performed numerically within the scheme described in Ref. [38].

The geometry optimizations of ZnS and NiO were performed by calculating the total energy for seven lattice parameters, spanning $\pm7\%$ around the experimental value, and fitting the calculated energies to the Birch-Murnaghan equation of state [54]. To optimize the geometry of TiO$_2$ (which is a function of three independent parameters), we fixed two of the parameters at their previous "best" values and calculated the energy as a function of the third, which we varied by $\pm7\%$ around the experimental value. After fitting a polynomial to the total energy we obtained a new "best" value for this parameter. We repeatedly cycled through all the parameters until no change was observed between iterations. For consistency we used this procedure for the EXX, RPA$+$EXX, and PBE$+U$ calculations, even though geometry optimization for the latter can be achieved more easily using the stress theorem [55].

For the heat of formation calculations, we modeled the O$_2$ molecule in its triplet state with a fixed bond length of 1.21 Å. We used periodic simulation cells and sampled the wave functions at the Γ point. For the calculation of $E_0 + E_X$ we used a simulation cell of size $12\times12\times13$ Å^3, and a cell of size of $6\times6\times7$ Å^3 for E_C^{RPA}.
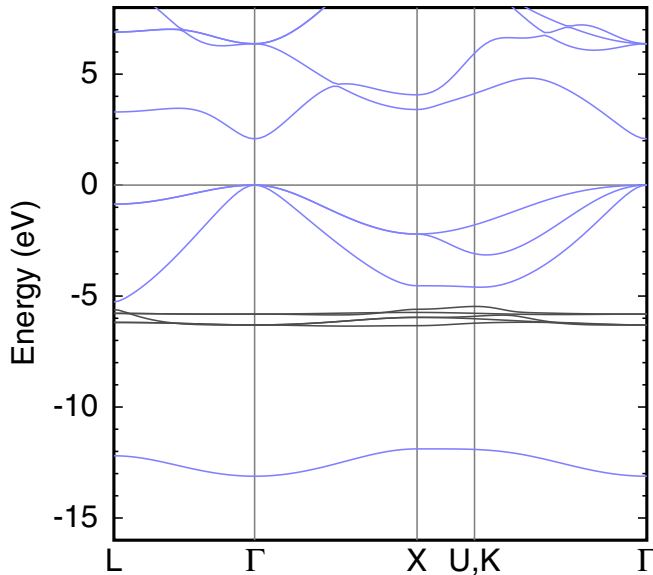
FIG. 1. Electronic band structure of sphalerite ZnS calculated at the experimentally measured lattice constant [56] using the PBE XC functional (no U correction). The energy zero has been set to the top of the valence band. The 3d band originating from the Zn atoms is located at -6 eV and highlighted in black.

FIG. 2. Lattice constant a of sphalerite ZnS calculated using total energies obtained self-consistently with the PBE XC functional and Hubbard-U correction (red), or non-self-consistently starting from PBE $+ U$ wave functions and eigenvalues including exact exchange without (green) and with (blue) the RPA correlation energy, as a function of U. The lines are guides to the eye. The lattice constant measured in Ref. [56] is shown as a gray horizontal line.

III. RESULTS AND DISCUSSION

A. ZnS

1. Electronic structure

We begin our study by considering ZnS in its sphalerite form (zinc blende, $F\bar{4}3m$). The electronic band structure calculated using the PBE XC functional is shown in Fig. 1. As found in numerous previous LDA/GGA calculations [57–62] the filled Zn-3d shells form a narrow band at 6 eV below the valence band edge. This 3d band is also observed in valence photoemission experiments, but at a larger binding energy of 9 eV [63,64].

Adding a Hubbard-U correction to the PBE XC-functional shifts the 3d band to larger binding energy, with the magnitude of the shift depending linearly on U. We find the 3d band position to coincide with the experimental binding energy when $U \approx 8$ eV. This value is consistent with two previous LDA $+ U$ studies [10,57] which required $(U_H - J)$ values of 9 and 7 eV to shift the 3d band to the experimentally observed position. Like these studies [10,57] we also observe that the band gap depends weakly on U, increasing from 2.1 to 2.6 eV when U is varied from 0 to 10 eV.

2. Atomistic structure

In Fig. 2 we show the equilibrium lattice constant calculated as a function of U, either at the PBE $+ U$ level or from the non-self-consistent RPA $+$ EXX and EXX total energies calculated from Eqs. (8) and (9). We compare our calculations to the value of 5.401 Å measured from x-ray diffraction [56] (horizontal line in Fig. 2). Considering the PBE $+ U$ calculations first (red line), at $U = 0$ eV we observe a lattice constant which is 0.8% larger than the reported experimental value. This difference is maintained over the U range of 0–6 eV and then
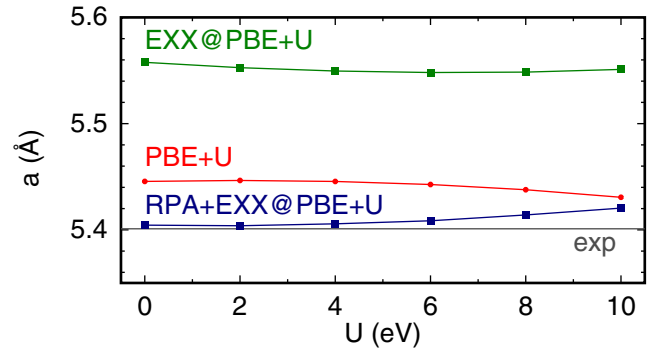
slightly decreases, to 0.5% for $U = 10$ eV. This magnitude of variation is rather small compared to the other materials discussed below, which we attribute to the energetic separation of the 3d bands. The other bands, lying 0–5 and 12–13 eV below the valence band maximum (VBM), have predominantly S-3p/Zn-4s and S-3s character, respectively. We note that for large values of U the Zn-3d band is pushed down in energy sufficiently to begin to hybridize with the S-3s states. Indeed fixing the lattice constant and monitoring the band character as a function of U shows a rapid increase in the Zn-3d contribution to the S-3s band for values of $U \geqslant 8$ eV.

Next considering the lattice constants obtained from the non-self-consistent exact exchange energy $E_{\text{Tot}}^{\text{EXX}}$ (green line in Fig. 2), we find a value 2.9% larger than experiment at $U = 0$ eV. This difference varies by less than 0.2% over the full range of U values. Although EXX lattice constants are often overestimated with respect to experiment [22], 2.9% is somewhat larger than the mean absolute error of 1.2% obtained in Ref. [22] for a test set of 20 semiconductors, which included several zinc blende structures. The correlation contribution to the total energy should therefore be considered particularly important to the bonding of ZnS.

Finally we consider lattice constants obtained after adding the non-self-consistent RPA correlation energy to the EXX energy, $E_{\text{Tot}}^{\text{RPA}}$ (blue line). Here we find lattice constants very close to the experimental value: 5.40 and 5.42 Å at $U = 0$ and 10 eV, corresponding to increases of <0.1% and 0.4%, respectively. The variation of lattice constant with U displays the opposite trend to the PBE $+ U$ calculations; in fact, the behavior is almost a perfect mirror image. That is, the XC interaction which favors increased bonding at high U within the PBE $+ U$ approximation is not present within the RPA description of the correlation energy.

Overall, our results show that the calculated lattice constant of sphalerite ZnS is somewhat insensitive to the value of U used in H^0, at all levels of theory. The fact that the Zn-3d states are already fully occupied and located deep below the VBM for $U = 0$ eV means that adding a U correction to these orbitals has a minimal effect on the ground-state electron density.
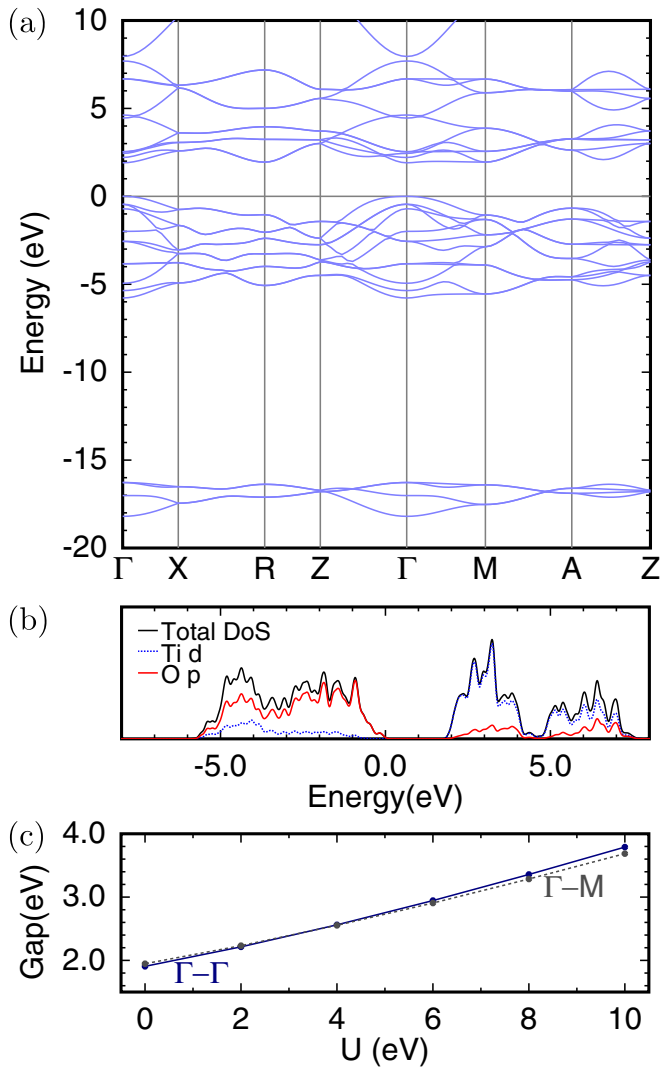
FIG. 3. (a) Electronic band structure of rutile TiO_2 calculated at the experimental structure [65] using the PBE XC functional (c.f. Fig. 1). (b) Density of states (DoS) of rutile around the valence and conduction band (black line) projected onto the Ti-d and O-p PAW projector functions (blue and red lines). (c) Evolution of the energy gaps with Hubbard-U correction applied to Ti-$3d$ states, corresponding to the direct transition at the Γ point ($\Gamma - \Gamma$, blue solid line) and the indirect transition ($\Gamma - M$, gray dotted line).

B. TiO_2

1. Electronic structure

We now consider TiO_2, a material where the $3d$ shell is largely unoccupied. The most naturally abundant forms of TiO_2 are the rutile (P4$_2$/mnm) and anatase (I4$_1$/amd) polymorphs [66]. We begin by focusing on rutile TiO_2, and calculate the electronic band structure and projected density of states (PDoS) at the PBE level using experimental structural parameters [65]. The results are shown in Figs. 3(a) and 3(b). The valence and conduction bands are formed from a mix of O-$2p$ and Ti-$3d$ states, with O-$2p$ dominating the valence band and vice versa. The Ti-$3d$ states in the conduction band are further split by the crystal field into t_{2g} and e_g subbands, over the energy region 2–4.5 eV and 4.5–7.5 eV above the

VBM. The O-$2s$ states lie far (17 eV) below the VBM. These electronic structure features have been observed and discussed in numerous other works [67–72].

The effect of including a Hubbard-U correction to the Ti-$3d$ states is to reduce the hybridization with the O-$2p$ orbitals in the conduction and valence bands, and to push the t_{2g} subband up in energy [72]. The latter phenomenon leads to a strong dependence of the fundamental gap on U [72,73], illustrated in Fig. 3(c). The direct gap at the Γ point increases by almost 2 eV over the U range of 0–10 eV, 4 times larger than observed for ZnS. As also shown in Fig. 3(c) the small difference between the direct gap at Γ and the $\Gamma - M$ transition (0.04 eV at $U = 0$ eV) reduces to zero at $U = 4$ eV, such that the nature of the fundamental gap changes from direct to indirect for $U \geqslant 4$ eV [73].

2. Atomistic structure

The structure of rutile TiO_2 is fully specified by the lattice parameters a and c and a dimensionless internal parameter u. Equivalently the structure may be described [74] in terms of distorted TiO_6 octahedra characterized by apical and equatorial bond lengths (d_{ap} and d_{eq}) and an angle θ, where 2θ is the smallest Ti–O–Ti angle in a given OTi$_3$ planar unit. The two parameter sets are related through

$$d_{ap} = ua\sqrt{2}, \tag{12}$$

$$d_{eq} = \frac{a}{2}\sqrt{\left(\frac{c}{a}\right)^2 + 8\left(\frac{1}{2} - u\right)^2}, \tag{13}$$

$$\cos 2\theta = \frac{2a^2\left(u - \frac{1}{2}\right)^2 - \frac{c^2}{4}}{2a^2\left(u - \frac{1}{2}\right)^2 + \frac{c^2}{4}}. \tag{14}$$

The inversions of Eqs. (12)–(14) are given in Ref. [74].

Figure 4 shows the calculated values of the parameters d_{ap}, d_{eq}, and 2θ as a function of U using PBE + U, and non-self-consistent EXX and RPA + EXX total energies. We also show the structural parameters obtained in the neutron diffraction experiments of Ref. [65], corresponding to $a = 4.587$ Å, $c = 2.954$ Å, and $u = 0.3047$. Considering the PBE + U data first, there is a strong dependence of the three parameters on the value of U used. d_{eq} and d_{ap} increase by 1.8% and 1.3% between $U = 0$ and 10 eV, which is a much larger change than the 0.3% decrease in Zn-S bond length observed for ZnS. A simple explanation for the observed lengthening of bonds is that the U correction makes the orbitals more atomiclike, reducing the hybridization shown in Fig. 3(b) and thus weakening the bonding [72]. The increased U also drives 2θ away from 90° and towards 120°, which as noted in Ref. [74] is its optimal value from the point of view of the planar threefold coordination of the O atoms; that is, the importance of the O atoms to the bonding increases with U.

Moving onto the EXX calculations, we see that d_{ap} and 2θ are effectively independent of U. d_{ap} is particularly close (<0.1%) to the experimental value, while 2θ is overestimated by 0.8%. However, d_{eq} displays a monotonic U dependence, with deviation from the experimental value varying from -1% to <0.1% for U between 0 and 10 eV. We note that the variation of E_{Tot}^{EXX} with U can only be due to the change in the shape
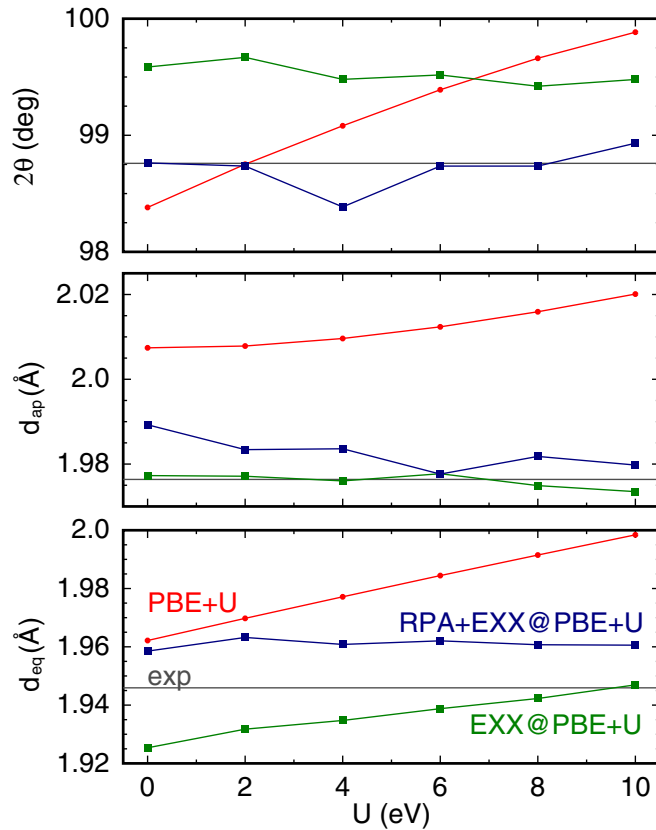
FIG. 4. Structural parameters of rutile TiO_2 calculated under different approximations (c.f. Fig. 2 for labels). The meaning of the three parameters is given in the main text. The experimental structural parameters (gray horizontal lines) were measured in Ref. [65].

of the occupied orbitals, which determines E_0 and E_X. We also note that the EXX structural parameters are closer to experiment than found for ZnS. This result is consistent with Refs. [66,69], which found the structures calculated within the Hartree-Fock approximation (self-consistent EXX) to be close to experimental values.

Given the apparent sensitivity of the EXX calculations of d_{eq} to the U value used, we might also expect the RPA + EXX structural parameters to exhibit a U dependence. In particular, since the denominator of χ_{KS} in Eq. (7) consists of energy differences between occupied and unoccupied states, the increase in band gap shown in Fig. 3(c) should introduce an additional coupling between $H^0(U)$ and E_{Tot}^{RPA}. What we observe, however, is that the RPA + EXX calculations are rather insensitive to the value of U used (blue lines in Fig. 4). Furthermore, the calculated structures are close to experiment; at $U = 0$ eV we find values of 4.616 Å, 2.973 Å, and 0.3047 for a, c, and u, which are all within 0.7% of experiment. There is noticeable noise in the data, particularly for the calculated 2θ, which reflects the difficulty in fitting the RPA total energy to three parameters. However, it is clear that calculating the total energy in the RPA + EXX scheme removes the strong U dependence observed in the PBE + U (and EXX) structural parameters, despite the implicit relation with U through ψ and ε.

3. Relative stability of rutile and anatase phases

An interesting property of TiO_2 is the competing stability of the rutile and anatase polymorphs. In nanostructured TiO_2 employed in photovoltaics, anatase tends to be the dominant phase [75]. However, the majority of experimental studies now agree that for bulk crystalline TiO_2, rutile is more thermodynamically stable than anatase, with reported enthalpy differences ranging[1] between 0.004 and 0.068 eV/formula unit (f.u.) [76]. Two recent experiments [76,77] found similar enthalpy differences of 0.027 and 0.017 eV/f.u. The measurement of this quantity is a significant experimental challenge, requiring careful control of impurity concentration and synthesis conditions [76].

A number of theoretical works have calculated the relative total energies of the anatase and rutile phases within DFT, e.g., Refs. [66,69,72,74,78–83]. Approaches using LDA or GGA XC functionals invariably determine anatase to have a lower total energy than rutile [66,69,80]. Our own calculations using the PBE XC functional and experimental geometries for the two phases [65] reproduce this result, with an energy difference of 0.077 eV/f.u.; using optimized geometries slightly increases this value to 0.080 eV/f.u. Inclusion of exact exchange through hybrid XC functionals also predicts anatase to have a lower energy [78,79], unless an unusually large amount ($>70\%$) of exact exchange is used [78].

In common with most previous works, we note that our calculations are missing the vibrational contribution to the total energy; however, the zero point contribution was calculated to be only 0.01 eV/f.u. lower for rutile than anatase in Ref. [80].[2] However, it has been shown that rutile can be significantly stabilized with respect to anatase within a DFT framework through two distinct routes, namely by adding either Hubbard-U terms to H^0 (GGA + U) [72,78] or empirical corrections to account for dispersion interactions (DFT-D) [81–83]. We note that even though both of these approaches can be used to obtain the same qualitative result, they describe very different physics; GGA + U addresses strong, localized correlation, while DFT-D attempts to capture relatively weak, long-range dispersion. The advantage of our current RPA approach is that it combines the Hubbard-U term with the RPA description of long-range correlation.

The red symbols in Fig. 5 show the relative energies of anatase with respect to rutile within the PBE + U approach. The filled and empty symbols correspond to optimized and experimental geometries, respectively. In agreement with previous studies [72,78], we find that increasing the U parameter stabilizes rutile, with the two phases becoming energetically degenerate at $U \sim 5.5$ eV. The authors of Ref. [72] further considered the columbite phase of TiO_2, and noted that U values in the range 5–8 eV gave an energy ordering which matches the relative stability from experiment. Although these large U values give band gaps close to experiment [73], they are somewhat larger than those calculated in Ref. [84] or used, e.g., in defect calculations [85].

---

[1]We exclude a value of 0.086 eV/f.u. listed in Ref. [76] due to its significant (71%) error bar.

[2]Interestingly Ref. [82] states that including the zero-point motion should stabilize anatase, at variance with Ref. [80].
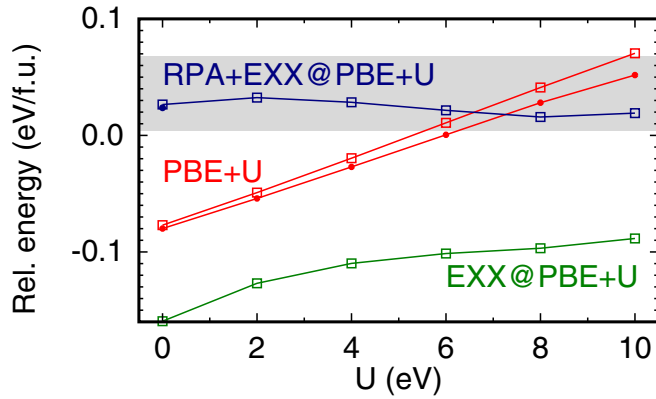
FIG. 5. Total energy per formula unit of the anatase phase of TiO_2 given with respect to the rutile phase. Open symbols denote calculations performed at the experimentally measured structures [65], and filled symbols using the structures optimized at the relevant level of theory. The lines are guides to the eye. We also illustrate the range of experimentally measured enthalpy differences between anatase and rutile (see text) [76] as the gray shaded area.

Following the same approach as for the structural parameters, we considered the difference between the anatase and rutile total energies calculated non-self-consistently including the EXX and RPA + EXX contributions. The EXX calculations (green symbols in Fig. 5) find anatase to have lower total energy than rutile regardless of the value of U used in the starting Hamiltonian. This result is consistent with previous Hartree-Fock calculations [66,69,74]. However, the RPA + EXX calculations (blue symbols in Fig. 5) show two interesting features: First, even at $U = 0$ eV, rutile has a lower energy than anatase, by 0.027 eV/f.u. Second, increasing U causes a nonmonotonic variation in this difference only up to a maximum of 0.011 eV/f.u. Thus, regardless of the U value used in the initial Hamiltonian, our calculated non-self-consistent RPA total energy of rutile remains lower than that of anatase.

Since these RPA + EXX calculations were performed at the experimental lattice parameters [65], we checked the energy difference obtained using RPA + EXX optimized structures[3] for $U = 0$ eV, and found a difference of only 0.003 eV/f.u. (filled blue symbol in Fig. 5). This is the same difference observed between experimental and optimized structures calculated within PBE + U at $U = 0$ eV. The difference, however, is that the RPA optimized structures depend less strongly on U than in PBE + U (Fig. 4), so we expect that using RPA + EXX optimized structures across the full U range to have an even smaller effect than that observed for the PBE + U calculations.

Comparing our total-energy calculations to the experimental enthalpy differences, we find our calculations to lie within the experimental range (shaded area of Fig. 5). We note that energy differences of <10 meV/f.u. lie at the limit of numerical accuracy currently achievable in our RPA
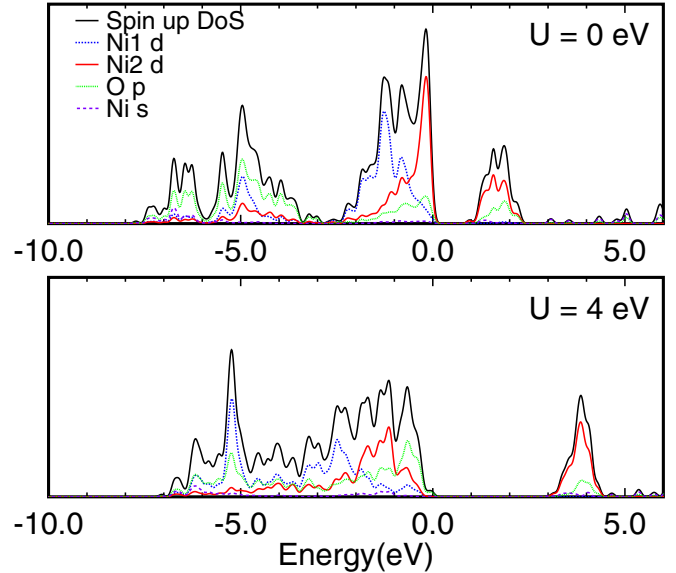

FIG. 6. Projected DoS calculated for NiO at the experimental lattice constant [86] using the PBE XC functional with and without a U correction of 4 eV. We consider one spin direction, and use the labels Ni1 and Ni2 to refer to the atoms with the majority of spins polarized parallel and antiparallel to this direction, respectively.

calculations, and again emphasize that our calculations do not include vibrational contributions. However, by comparing the RPA + EXX and EXX total energies in Fig. 5 it can be seen that the RPA correlation energy of rutile is more negative than that of anatase by 0.186 eV/f.u. at $U = 0$ eV, and by 0.108 eV at $U = 10$ eV. Therefore, our calculations illustrate the key role played by nonlocal correlation in understanding the phase stability of this material [81], and also demonstrate that the result is robust against the choice of U in $H^0(U)$.

C. NiO

1. Electronic structure

The final material we consider is NiO, which in its paramagnetic state adopts a NaCl ($Fm\bar{3}m$) structure [86]. Here we focus on the antiferromagnetic configuration formed below the Néel temperature (523 K), where the spin direction alternates between adjacent (111) Ni planes. For simplicity we neglect the structural distortion which accompanies this antiferromagnetic transition, since the deviation from the cubic lattice is small (<0.1° angular variation in lattice vectors) [86].

In Fig. 6 we show the NiO PDoS resolved for one of the two spin components, calculated at the experimental lattice constant [86] (4.170 Å) at the PBE + U level for $U = 0$ and 4 eV. The PDoS demonstrates the complex character of the conduction and valence bands, which both contain a substantial proportion of Ni-3d states [7,9,11,48]. The effect of the U parameter is to open the gap between d states, which significantly increases the band gap from 1.0 eV at $U = 0$ eV to 3.0 eV at $U = 4$ eV. Furthermore, the character of the band edges changes, such that the valence band edge is dominated by O-2p states at $U = 4$ eV (Fig. 6). The ground-state spin density is also strongly U dependent, with the magnitude of the local magnetic moment on the Ni atoms increasing from 1.4 to
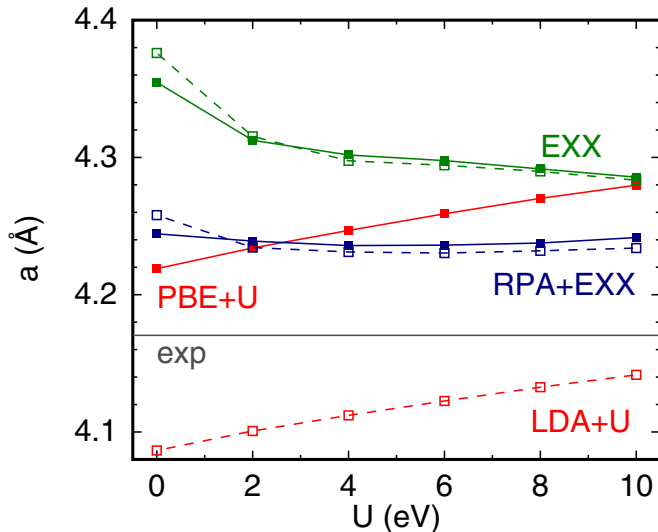
_____

[3]The experimental [65] (RPA + EXX optimized) lattice parameters for anatase TiO_2 at $U = 0$ eV used were $a = 3.782$ Å (3.812 Å), $c = 9.502$ Å (9.567 Å) and $u = 0.2083$ (0.2083).

FIG. 7. Lattice constant a of NiO calculated under different approximations (c.f. Fig. 2 for labels). Filled and empty symbols correspond to PBE $+ U$ and LDA $+ U$ calculations, respectively. The experimental lattice constant (gray horizontal line) was measured in Ref. [86].

1.8 Bohr magnetons (μ_B) over a U range of 0–10 eV [47]. It is also interesting to note that both the gap and local magnetic moment exhibit variation between the LDA (0.4 eV and $1.2\mu_B$) and PBE (1.0 eV and $1.4\mu_B$) with $U = 0$ eV.

2. Atomistic structure

Given the strong U dependence of the ground-state density, we would expect the lattice constant of NiO also to be sensitive to U. Figure 7 shows that this is indeed the case when the total energy is obtained at the PBE $+ U$ or LDA $+ U$ level (red symbols), with the lattice expanding for increased U. Reference [9] noted that this expansion was accompanied by a decrease in electronic charge in the interstitial regions, i.e., a reduction in covalent bonding. Our calculated variation of LDA/PBE $+ U$ lattice constants with U in the range 0–6 eV (0.04 Å) is smaller than that reported in Ref. [9] (0.11 Å) but larger than Ref. [48] (<0.01 Å). We attribute this difference to the frozen core approximation/core-valence partitioning used in the PAW datasets. The LDA and PBE calculations display the usual trend [87] of underestimating and overestimating the experimental lattice constant [86], respectively, (-2.0% and $+1.1\%$ at $U = 0$ eV).

The lattice constant calculated from $E_{\mathrm{Tot}}^{\mathrm{EXX}}$ with PBE wave functions overestimates the experimental value by 4.4%. This non-self-consistent value exhibits poorer agreement with experiment than that obtained from Hartree-Fock calculations in Ref. [9], which overestimated the experimental value by 2.1%. Initially, on including a U correction of 2 eV there is a relatively large decrease in lattice constant (0.04 Å), but for higher U values the dependence is weaker (<0.03 Å between $U = 2$ and 10 eV). Furthermore, apart from a difference of 0.02 Å at $U = 0$ eV, using LDA $+ U$ wave functions to calculate $E_{\mathrm{Tot}}^{\mathrm{EXX}}$ yields very similar results to PBE $+ U$ (green dashed lines in Fig. 7).

The non-self-consistent RPA total-energy calculations based on PBE $+ U$ wave functions (blue solid line in Fig. 7)

overestimate the experimental lattice constant by 1.6%–1.7% over the entire range of U values. The lattice constants obtained starting from LDA $+ U$ (blue dashed lines) display the same trend as the EXX calculations, i.e., a larger difference at $U = 0$ eV compared to all other U values. In general the agreement with experiment is not as good as found for the RPA calculations for TiO_2 and ZnS, and the PBE ($U = 0$ eV) lattice constant is closer to experiment. Reference [88] similarly found PBE to give a more accurate lattice constant for elemental Ni than the RPA, with more recent work attributing the difference to the quality of PAW datasets [89]. However, the most important feature of Fig. 7 is that, like the other materials considered in this work, the non-self-consistent RPA structural parameters are largely insensitive to the value of U used in the initial Hamiltonian. This perhaps is all the more remarkable for NiO, given the strong U dependence of the spin density, band edge character, and gap.

D. U dependence of total energy

In order to further understand the effects of $H^0(U)$ on the calculated value of $E_{\mathrm{Tot}}^{\mathrm{RPA}}$, in Fig. 8 we plot the individual contributions E_0, E_{X}, and $E_{\mathrm{C}}^{\mathrm{RPA}}$ as a function of U for each material at their experimental structures (for TiO_2 we show the results for the rutile phase). The energies were calculated starting from PBE $+ U$ wave functions, and the $U = 0$ eV value of each quantity has been used to define the energy zero.

The most notable aspect of Fig. 8 is that although E_0, E_{X}, and $E_{\mathrm{C}}^{\mathrm{RPA}}$ are in general strongly U dependent (varying by several eV/f.u. over the considered U range), the variation in their sum $E_{\mathrm{Tot}}^{\mathrm{RPA}}$ is an order of magnitude smaller; i.e., there is a strong cancellation between the U-dependent quantities. In all cases, E_{X} becomes more negative with increasing U. A simple explanation for this behavior is to note that the larger U correction forces the electrons to occupy more atomiclike orbitals, increasing the self-interaction contribution to E_{X} [the $\nu_1 = \nu_2$ term in Eq. (4)].

The contributions which cancel E_{X} vary from material to material. For ZnS, the E_{X} contribution is mainly balanced by E_0, while for TiO_2 it is $E_{\mathrm{C}}^{\mathrm{RPA}}$. In NiO both E_0 and $E_{\mathrm{C}}^{\mathrm{RPA}}$ contribute. The behavior of E_0 with U depends on whether the $3d$ states are occupied (ZnS, NiO) or mainly unoccupied (TiO_2). In the former case, the U term causes the $3d$ states to become more localized, which carries a kinetic energy penalty and thus increases E_0. By contrast for TiO_2, the U correction depopulates the $3d$ states and pushes these electrons into the less-localized $2p$ orbitals, reducing the kinetic contribution.

The RPA correlation energy $E_{\mathrm{C}}^{\mathrm{RPA}}$ becomes more positive (i.e., decreases in magnitude) with increasing U. The principal cause of this behavior is the increase in band gap, which reduces the screening through the energy denominators in χ_{KS} [Eq. (7)]. The increased variation of $E_{\mathrm{C}}^{\mathrm{RPA}}$ across ZnS $\rightarrow$ $TiO_2 \rightarrow$ NiO reflects the sensitivity of the material's band gap to U. However, the observed behavior of $E_{\mathrm{C}}^{\mathrm{RPA}}$ cannot be viewed entirely in terms of the band gap. To illustrate this point, in Fig. 8 for TiO_2 we show the correlation energy calculated using the PBE ($U = 0$ eV) wave functions, where the effect of U on the band gap was mimicked by applying a scissor correction to the unoccupied states used to construct χ_{KS}. Specifically, the size of the scissor correction was related
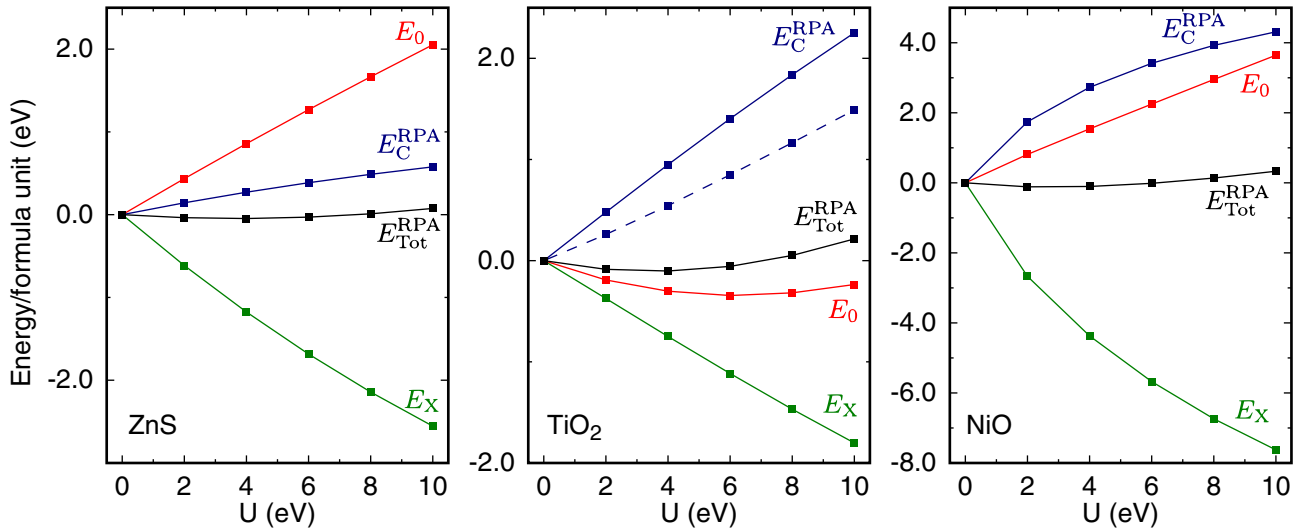
FIG. 8. Decomposition of $E_{\mathrm{Tot}}^{\mathrm{RPA}}$ into its individual contributions [Eq. (8)] as a function of the U parameter used in initial PBE + U calculation. Each quantity is given with respect to its calculated value at $U = 0$ eV. The dashed line shown for TiO$_2$ shows $E_{\mathrm{C}}^{\mathrm{RPA}}$ calculated with the effects of U simulated with a scissor correction (see text).

to U through Fig. 3(c) to reproduce the Γ-Γ gap. As shown by the dashed line in Fig. 8, the scissor correction accounts for $\sim 65\%$ of the variation in $E_{\mathrm{C}}^{\mathrm{RPA}}$. In order to account for the remaining 35% it is therefore necessary to also consider the U-dependent variations of the band structure (e.g., the position of the e_g and t_{2g} subbands) and the shapes of the wave functions.

In Fig. 9 we compare the magnitude of variation of $E_{\mathrm{Tot}}^{\mathrm{RPA}}$ with the self-consistent total energy obtained with the PBE + U XC functional. The metals Ti and Ni are included in this analysis; these calculations are discussed in more detail in Sec. III F below. Comparison of the scales on the y axis emphasizes how the self-consistent PBE + U energy is much more sensitive to U than $E_{\mathrm{Tot}}^{\mathrm{RPA}}$. In the case of TiO$_2$, this difference is a factor of 30. A further interesting point regarding TiO$_2$ is the energy difference between the anatase and rutile polymorphs shown in Fig. 5. Here we see that the variation in energy difference between the two polymorphs, going from -0.08 to 0.07 eV/f.u. over the U range of 0–10 eV, is 40

times smaller than the variation in the self-consistent PBE + U energy of each phase. By contrast the variation in $E_{\mathrm{Tot}}^{\mathrm{RPA}}$ is the same order of magnitude as the energy difference.

E. Minimization of $E_{\mathrm{Tot}}^{\mathrm{RPA}}$ with $H^0(U)$

Interestingly, Fig. 9 also demonstrates that it is possible to minimize $E_{\mathrm{Tot}}^{\mathrm{RPA}}$ with respect to the continuum of single-particle Hamiltonians $H^0(U)$ defined by U, and thus introduce a material-dependent quantity $U_{\min}$ at which $E_{\mathrm{Tot}}^{\mathrm{RPA}}$ is a minimum. It is shown in Ref. [42] that a blind optimization of $E_{\mathrm{Tot}}^{\mathrm{RPA}}$ with respect to all possible H^0 (where H^0 contains a nonlocal potential) will push all eigenvalues to the Fermi level and thus cause $E_{\mathrm{Tot}}^{\mathrm{RPA}} \to -\infty$. In the same work it is suggested that a sensible method of proceeding is to somehow constrain H^0 so as to avoid this unphysical behavior. The current work can be seen as an implementation of this idea, where specifically we have restricted our search to Hamiltonians of the form $H^0(U)$ [Eq. (11)].
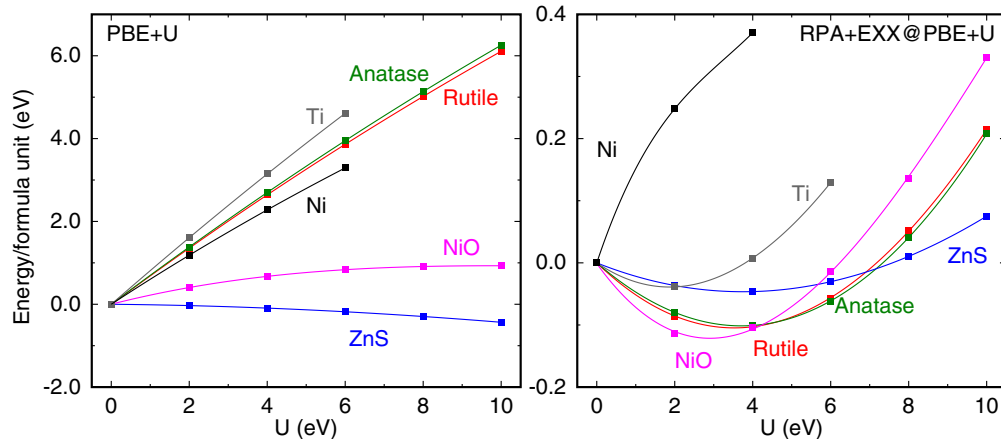

FIG. 9. Total energies per formula unit as a function of U, calculated (left) self-consistently from the PBE + U XC functional, and (right) non-self-consistently from Eq. (8). Both the rutile and anatase TiO$_2$ polymorphs are considered. Each quantity is given with respect to its calculated value at $U = 0$ eV. The lines are polynomial fits to the calculated data points (squares).

TABLE II. Values of U_{min} obtained for the materials considered in this work. U_{min} is determined from Fig. 9 as the U value at which each curve is at a minimum. We compare our results to U values reported from previous calculations.

	U_{min} (eV)	Previously calculated U (eV)
ZnS	3.7	6.0[a], 7.0[b]
TiO$_2$ (rutile)	3.5	3.4[c], 6.0[d]
TiO$_2$ (anatase)	3.7	3.3[c], 5.3[d], 7.5[e]
NiO	2.9	7.1,[f] 4.6,[g] 6.2,[h] 6.4[i]
Ti	1.8	–
Ni	–	–

[a]$U_H - J$, constrained DFT, Ref. [10].
[b]Matrix elements of screened Coulomb interaction, Ref. [57].
[c]Linear response formalism, Ref. [84].
[d]Linear response formalism, Ref. [78].
[e]Matching of G_0W_0 and PBE $+ U$ band gap, Ref. [73].
[f]Constrained DFT, Ref. [7].
[g]Linear response formalism, Ref. [11].
[h]Fit to experimental electron energy loss spectrum, Ref. [9].
[i]Fit to experimental heat of formation, Ref. [90].

In Table II we compare our obtained U_{min} to other values of U used in previous works. Although it is less common to apply U corrections to metals [91], standard PBE $+ U$ calculations of heats of formation find it necessary to apply the Hubbard U also to the metallic system, with reasonable results [14]. Our numbers are generally smaller than those used in other works; of course, given our unique criterion of determining U_{min}, there is no reason why they should agree. Indeed the value of U depends on the choice made for the projector functions [8], and can vary on the scale of electronvolts depending on the treatment of the core-valence interaction [78].

We note that the values of U_{min} obtained here give reasonable physical properties, such as a local magnetic moment of 1.6 μ_B for NiO (experimental values range from 1.6–1.9 μ_B) [11]. However, it is also true that the computational cost of obtaining U_{min} does not make the above scheme an attractive method of selecting U compared to other methods [7,11]. Indeed, the quite weak sensitivity of the energy to the value of U combined with the numerical uncertainty inherent in such calculations means that we must attach caution to the values listed in Table II. Nonetheless it would be interesting to explore the minimization of E_{Tot}^{RPA} with respect to $H^0(U)$ for an extended range of TMCs.

F. Heats of formation of TiO$_2$ and NiO

A recent work [14] presented calculations of the heats of formation for a range of oxides, allowing comparison of the performance of different total-energy methods, including the non-self-consistent RPA. TiO$_2$ (rutile) and NiO were among the materials considered in Ref. [14], and are notable because of the very good (TiO$_2$) and very poor (NiO) agreement found between their calculated heats of formation and experiments. To make contact with that work, we also calculated the heats of formation, obtained per oxygen atom as

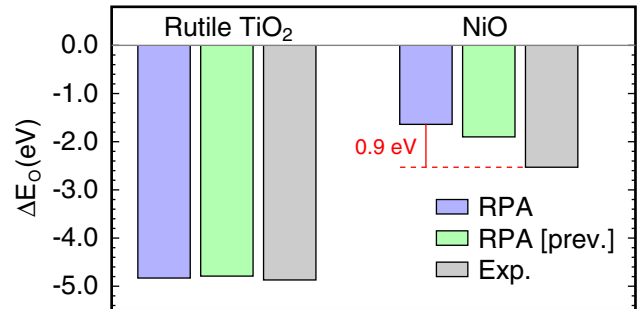$$\Delta E_O = \frac{1}{y}E(A_xO_y) - \frac{x}{y}E(A) - \frac{1}{2}E(O_2), \quad (15)$$

FIG. 10. Heat of formation per oxygen atom ΔE_O calculated from Eq. (15). Blue and green bars represent non-self-consistent RPA total-energy calculations performed using PBE wave functions in the current and previous (prev.) work [14]. Gray bars represent experimental values [14].

where $E(A_xO_y)$, $E(A)$, and $E(O_2)$ are the energies per formula unit of the oxide, metal, and oxygen molecule, respectively. We used experimental lattice parameters throughout, with Ti in an hcp structure ($P6_3/mmc$), $a = 2.957$ Å, and $c/a = 1.585$ [92], and (ferromagnetic) Ni in a fcc structure (F$m\bar{3}m$) with $a = 3.516$ Å [93].

The values of ΔE_O for TiO$_2$ and NiO calculated from E_{Tot}^{RPA} (PBE wave functions, $U = 0$ eV) are presented in Fig. 10. We compare our results to the calculations and room temperature experimental values reported in Ref. [14]. Focusing first on the calculations, we find good agreement (0.04 eV) between our ΔE_O and that of Ref. [14] for TiO$_2$. However, there exists a difference of 0.3 eV in ΔE_O for NiO, which we assign to our explicit treatment of the Ni $3p$ states. If instead these states are frozen in the Ni core we obtain a value of ΔE_O of -1.84 eV, much closer to the -1.90 eV reported in Ref. [14]. We also note that Ref. [14] used PBE structural parameters, while here we use experimental values; this aspect also explains the difference in ΔE_O for rutile TiO$_2$ calculated here and in Ref. [15].

Now considering experiment, for rutile TiO$_2$ there is close agreement with the non-self-consistent RPA with a difference in ΔE_O of 0.04 eV. However, as emphasized in Fig. 10, for NiO there is a significant discrepancy (0.9 eV), with the non-self-consistent RPA apparently underestimating the stability of NiO compared to Ni. Reference [14] found similarly poor performance for the monoxides VO and CoO, and Cr$_2$O$_3$.

In the context of the current work it is natural to ask whether one can obtain RPA values of ΔE_O closer to experiment by including a U correction in the initial Hamiltonian. This approach can be tested immediately from the data shown in Fig. 9. Choosing the U value as U_{min} would shift ΔE_O to more negative values for both TiO$_2$ and NiO. For TiO$_2$ the new ΔE_O is 0.03 eV lower in energy, essentially reproducing the experimental value (although no vibrational effects were taken into account in the calculations). For NiO, the correction is -0.12 eV which, although slightly reducing the discrepancy with experiment, does not account for the 0.9-eV difference.

NiO has long been recognized as a system representing a major challenge to density-functional-based methods [7], and we also note that metallic Ni cannot be considered straightforward either [94]. One option is to go beyond the RPA in the

calculation of the correlation energy, for instance, through the introduction of a time-dependent DFT kernel in the integral equation for $\chi^{\lambda}(\omega)$ [95]. Recently it was found that such an approach employing a static kernel based on the homogeneous electron gas reduced the absolute error in ΔE_O by 0.2 eV for a range of metal oxides, compared to the RPA [15]. Further exploration of kernels which have a frequency dependence or display a small-wave-vector divergence [87] would be an interesting direction for future study.

IV. CONCLUSIONS

We have presented a study into the effects of including a Hubbard-U correction in the calculation of the single-particle wave functions used to construct the non-self-consistent exact exchange and RPA correlation energy. We have explored materials where the $3d$ band is fully occupied (ZnS), almost empty (TiO$_2$), and partly occupied (NiO), and determined the U dependence of their lattice constants. We have further addressed the question of the relative stability of the TiO$_2$ polymorphs anatase and rutile, and the heats of formation of the oxides TiO$_2$ and NiO.

The principal conclusion of this work is that the lattice constants derived from the non-self-consistent RPA total energy $E_{\mathrm{Tot}}^{\mathrm{RPA}}$ are remarkably robust against changes to the value of U in the starting Hamiltonian. NiO is a good example: Including a U correction opens the band gap, redistributes the spin density, and changes the character of the band edges, yet the non-self-consistent RPA lattice constant changes by less than 0.01 Å over U values ranging from 0–10 eV.

We have further shown that $E_{\mathrm{Tot}}^{\mathrm{RPA}}$ itself is far less sensitive to U than the self-consistent PBE $+ U$ total energy. This insensitivity originates from competing U dependencies of the noninteracting (E_0), exchange (E_{EXX}), and correlation ($E_{\mathrm{C}}^{\mathrm{RPA}}$) energies. For the materials considered here we have shown it is possible to minimize $E_{\mathrm{Tot}}^{\mathrm{RPA}}$ with respect to the U value by choosing the single-particle Hamiltonian $H^0(U = U_{\mathrm{min}})$.

For the specific case of TiO$_2$, we have found the difference in $E_{\mathrm{Tot}}^{\mathrm{RPA}}$ between rutile and anatase polymorphs to vary by less than 0.01 eV per formula unit over the entire U range. This variation is an order of magnitude smaller than that calculated self-consistently at the PBE $+ U$ level. Furthermore, the non-self-consistent RPA energy ordering reflects the ordering of experimental enthalpies.

The observed insensitivity of $E_{\mathrm{Tot}}^{\mathrm{RPA}}$ to H^0 should be considered a positive attribute of non-self-consistent RPA total-energy calculations of the structural properties of solids, and distinguishes the method from G_0W_0 calculations of quasiparticle energies which display a stronger starting point dependence. By the same token, however, situations which are problematic for the RPA based on GGA or LDA Hamiltonians are unlikely to be improved by attaching a U correction to H^0. We have demonstrated this explicitly in the case of the heat of formation of NiO, where the inclusion of U corrections can only reduce the discrepancy with experiment by a small amount. Such cases must therefore remain a challenge for beyond-RPA methods.

[1] B. O'Regan and M. Grätzel, Nature (London) **353**, 737 (1991).

[2] A. Fujishima and K. Honda, Nature (London) **238**, 37 (1972).

[3] R. H. Kodama, S. A. Makhlouf, and A. E. Berkowitz, Phys. Rev. Lett. **79**, 1393 (1997).

[4] M. Bruchez, M. Moronne, P. Gin, S. Weiss, and A. P. Alivisatos, Science **281**, 2013 (1998).

[5] P. Hohenberg and W. Kohn, Phys. Rev. **136**, B864 (1964).

[6] V. I. Anisimov, F. Aryasetiawan, and A. I. Lichtenstein, J. Phys.: Condens. Matter **9**, 767 (1997).

[7] V. I. Anisimov, J. Zaanen, and O. K. Andersen, Phys. Rev. B **44**, 943 (1991).

[8] W. E. Pickett, S. C. Erwin, and E. C. Ethridge, Phys. Rev. B **58**, 1201 (1998).

[9] S. L. Dudarev, G. A. Botton, S. Y. Savrasov, C. J. Humphreys, and A. P. Sutton, Phys. Rev. B **57**, 1505 (1998).

[10] H. Jiang, R. I. Gomez-Abal, P. Rinke, and M. Scheffler, Phys. Rev. B **82**, 045108 (2010).

[11] M. Cococcioni and S. de Gironcoli, Phys. Rev. B **71**, 035105 (2005).

[12] X. Ren, P. Rinke, C. Joas, and M. Scheffler, J. Mater. Sci. **47**, 7447 (2012).

[13] H. Eshuis, J. E. Bates, and F. Furche, Theor. Chem. Acc. **131**, 1084 (2012).

[14] J. Yan and J. K. Nørskov, Phys. Rev. B **88**, 245204 (2013).

[15] T. S. Jauho, T. Olsen, T. Bligaard, and K. S. Thygesen, Phys. Rev. B **92**, 115140 (2015).

[16] H. Peng and S. Lany, Phys. Rev. B **87**, 174113 (2013).

[17] J. Yan, J. S. Hummelshøj, and J. K. Nørskov, Phys. Rev. B **87**, 075207 (2013).

[18] L. Schimka, J. Harl, A. Stroppa, A. Grüneis, M. Marsman, F. Mittendorfer, and G. Kresse, Nat. Mater. **9**, 741 (2010).

[19] T. Olsen, J. Yan, J. J. Mortensen, and K. S. Thygesen, Phys. Rev. Lett. **107**, 156401 (2011).

[20] D. Lu, Y. Li, D. Rocca, and G. Galli, Phys. Rev. Lett. **102**, 206411 (2009).

[21] A. Marini, P. García-González, and A. Rubio, Phys. Rev. Lett. **96**, 136404 (2006).

[22] J. Harl, L. Schimka, and G. Kresse, Phys. Rev. B **81**, 115126 (2010).

[23] W. Kohn and L. J. Sham, Phys. Rev. **140**, A1133 (1965).

[24] N. L. Nguyen, N. Colonna, and S. de Gironcoli, Phys. Rev. B **90**, 045138 (2014).

[25] J. Klimeš and G. Kresse, J. Chem. Phys. **140**, 054516 (2014).

[26] M. Grüning, A. Marini, and A. Rubio, J. Chem. Phys. **124**, 154108 (2006).

[27] T. Kotani, J. Phys.: Condens. Matter **10**, 9241 (1998).

[28] R. W. Godby, M. Schlüter, and L. J. Sham, Phys. Rev. B **37**, 10159 (1988).

[29] M. S. Hybertsen and S. G. Louie, Phys. Rev. B **34**, 5390 (1986).

[30] N. Marom, F. Caruso, X. Ren, O. T. Hofmann, T. Körzdörfer, J. R. Chelikowsky, A. Rubio, M. Scheffler, and P. Rinke, Phys. Rev. B **86**, 245127 (2012).

[31] F. Fuchs, J. Furthmüller, F. Bechstedt, M. Shishkin, and G. Kresse, Phys. Rev. B **76**, 115109 (2007).

[32] F. Bruneval and M. A. L. Marques, J. Chem. Theor. Comput. **9**, 324 (2013).

[33] F. Caruso, P. Rinke, X. Ren, M. Scheffler, and A. Rubio, Phys. Rev. B **86**, 081102 (2012).

[34] H. Jiang and E. Engel, J. Chem. Phys. **127**, 184108 (2007).

[35] A. Grüneis, M. Marsman, J. Harl, L. Schimka, and G. Kresse, J. Chem. Phys. **131**, 154115 (2009).

[36] J. Toulouse, W. Zhu, J. G. Ángyán, and A. Savin, Phys. Rev. A **82**, 032502 (2010).

[37] J. G. Ángyán, R.-F. Liu, J. Toulouse, and G. Jansen, J. Chem. Theor. Comput. **7**, 3116 (2011).

[38] T. Olsen and K. S. Thygesen, Phys. Rev. B **87**, 075111 (2013).

[39] M. Casadei, X. Ren, P. Rinke, A. Rubio, and M. Scheffler, Phys. Rev. Lett. **109**, 146402 (2012).

[40] F. Caruso, D. R. Rohr, M. Hellgren, X. Ren, P. Rinke, A. Rubio, and M. Scheffler, Phys. Rev. Lett. **110**, 146403 (2013).

[41] M. Hellgren, F. Caruso, D. R. Rohr, X. Ren, A. Rubio, M. Scheffler, and P. Rinke, Phys. Rev. B **91**, 165110 (2015).

[42] S. Ismail-Beigi, Phys. Rev. B **81**, 195126 (2010).

[43] D. C. Langreth and J. P. Perdew, Phys. Rev. B **15**, 2884 (1977).

[44] O. Gunnarsson and B. I. Lundqvist, Phys. Rev. B **13**, 4274 (1976).

[45] M. Petersilka, U. J. Gossmann, and E. K. U. Gross, Phys. Rev. Lett. **76**, 1212 (1996).

[46] J. Yan, J. J. Mortensen, K. W. Jacobsen, and K. S. Thygesen, Phys. Rev. B **83**, 245122 (2011).

[47] J. Enkovaara *et al.*, J. Phys.: Condens. Matter **22**, 253202 (2010).

[48] A. Rohrbach, J. Hafner, and G. Kresse, Phys. Rev. B **69**, 075413 (2004).

[49] P. E. Blöchl, Phys. Rev. B **50**, 17953 (1994).

[50] J. P. Perdew and Y. Wang, Phys. Rev. B **45**, 13244 (1992).

[51] J. P. Perdew, K. Burke, and M. Ernzerhof, Phys. Rev. Lett. **77**, 3865 (1996).

[52] H. J. Monkhorst and J. D. Pack, Phys. Rev. B **13**, 5188 (1976).

[53] R. Sundararaman and T. A. Arias, Phys. Rev. B **87**, 165122 (2013).

[54] F. Birch, Phys. Rev. **71**, 809 (1947).

[55] O. H. Nielsen and R. M. Martin, Phys. Rev. B **32**, 3780 (1985).

[56] U. Hotje, C. Rose, and M. Binnewies, Solid State Sci. **5**, 1259 (2003).

[57] T. Miyake, P. Zhang, M. L. Cohen, and S. G. Louie, Phys. Rev. B **74**, 245213 (2006).

[58] P. Rinke, A. Qteish, J. Neugebauer, C. Freysoldt, and M. Scheffler, New J. Phys. **7**, 126 (2005).

[59] D. Vogel, P. Krüger, and J. Pollmann, Phys. Rev. B **54**, 5495 (1996).

[60] S. Z. Karazhanov, P. Ravindran, A. Kjekshus, H. Fjellvåg, and B. G. Svensson, Phys. Rev. B **75**, 155104 (2007).

[61] T. Kotani and M. van Schilfgaarde, Solid State Commun. **121**, 461 (2002).

[62] M. Shishkin and G. Kresse, Phys. Rev. B **75**, 235102 (2007).

[63] L. Ley, R. A. Pollak, F. R. McFeely, S. P. Kowalczyk, and D. A. Shirley, Phys. Rev. B **9**, 600 (1974).

[64] R. Weidemann, H.-E. Gumlich, M. Kupsch, H.-U. Middelmann, and U. Becker, Phys. Rev. B **45**, 1172 (1992).

[65] J. K. Burdett, T. Hughbanks, G. J. Miller, J. W. Richardson, and J. V. Smith, J. Am. Chem. Soc. **109**, 3639 (1987).

[66] J. Muscat, V. Swamy, and N. M. Harrison, Phys. Rev. B **65**, 224112 (2002).

[67] J. B. Goodenough, Prog. Solid State Chem. **5**, 145 (1971).

[68] K. M. Glassford and J. R. Chelikowsky, Phys. Rev. B **46**, 1284 (1992).

[69] F. Labat, P. Baranek, C. Domain, C. Minot, and C. Adamo, J. Chem. Phys. **126**, 154703 (2007).

[70] L. Chiodo, J. M. García-Lastra, A. Iacomino, S. Ossicini, J. Zhao, H. Petek, and A. Rubio, Phys. Rev. B **82**, 045207 (2010).

[71] W. Kang and M. S. Hybertsen, Phys. Rev. B **82**, 085203 (2010).

[72] M. E. Arroyo-de Dompablo, A. Morales-García, and M. Taravillo, J. Chem. Phys. **135**, 054503 (2011).

[73] C. E. Patrick and F. Giustino, J. Phys.: Condens. Matter **24**, 202201 (2012).

[74] A. Fahmi, C. Minot, B. Silvi, and M. Causá, Phys. Rev. B **47**, 11717 (1993).

[75] V. Shklover, M.-K. Nazeeruddin, S. M. Zakeeruddin, C. Barbé, A. Kay, T. Haibach, W. Steurer, R. Hermann, H.-U. Nissen, and M. Grätzel, Chem. Mater. **9**, 430 (1997).

[76] M. R. Ranade, A. Navrotsky, H. Z. Zhang, J. F. Banfield, S. H. Elder, A. Zaban, P. H. Borse, S. K. Kulkarni, G. S. Doran, and H. J. Whitfield, Proc. Natl. Acad. Sci. USA **99**, 6476 (2002).

[77] A. A. Levchenko, G. Li, J. Boerio-Goates, B. F. Woodfield, and A. Navrotsky, Chem. Mater. **18**, 6324 (2006).

[78] M. T. Curnan and J. R. Kitchin, J. Phys. Chem. C **119**, 21060 (2015).

[79] M. Gerosa, C. E. Bottani, L. Caramella, G. Onida, C. Di Valentin, and G. Pacchioni, Phys. Rev. B **91**, 155201 (2015).

[80] R. Shirley, M. Kraft, and O. R. Inderwildi, Phys. Rev. B **81**, 075111 (2010).

[81] J. C. Conesa, J. Phys. Chem. C **114**, 22718 (2010).

[82] J. Moellmann, S. Ehrlich, R. Tonner, and S. Grimme, J. Phys.: Condens. Matter **24**, 424206 (2012).

[83] T. Zhu and S.-P. Gao, J. Phys. Chem. C **118**, 11385 (2014).

[84] G. Mattioli, F. Filippone, P. Alippi, and A. Amore Bonapasta, Phys. Rev. B **78**, 241201 (2008).

[85] C. Dette, M. A. Pérez-Osorio, C. S. Kley, P. Punke, C. E. Patrick, P. Jacobson, F. Giustino, S. J. Jung, and K. Kern, Nano Lett. **14**, 6533 (2014).

[86] A. K. Cheetham and D. A. O. Hope, Phys. Rev. B **27**, 6964 (1983).

[87] C. E. Patrick and K. S. Thygesen, J. Chem. Phys. **143**, 102802 (2015).

[88] L. Schimka, R. Gaudoin, J. Klimeš, M. Marsman, and G. Kresse, Phys. Rev. B **87**, 214102 (2013).

[89] J. Klimeš, M. Kaltak, and G. Kresse, Phys. Rev. B **90**, 075125 (2014).

[90] L. Wang, T. Maxisch, and G. Ceder, Phys. Rev. B **73**, 195107 (2006).

[91] V. I. Anisimov and O. Gunnarsson, Phys. Rev. B **43**, 7570 (1991).

[92] Y. K. Vohra and P. T. Spencer, Phys. Rev. Lett. **86**, 3068 (2001).

[93] P. Haas, F. Tran, and P. Blaha, Phys. Rev. B **79**, 085104 (2009).

[94] F. Starrost, H. Kim, S. C. Watson, E. Kaxiras, and E. A. Carter, Phys. Rev. B **64**, 235105 (2001).

[95] T. Olsen and K. S. Thygesen, Phys. Rev. B **88**, 115131 (2013).